Astronomy & Astrophysics manuscript no. akarska
August 22, 2019

Working title

Agata Karska[1], Agnieszka Mirocha[1,2], Lars E. Kristensen[3], Marcin Gronowski[4], Miguel Figueira[5], Marcin Gładkowski[2,6], Michał Żółtowski[2], and Łukasz Tychoniec[7]

[1] Centre for Astronomy, Faculty of Physics, Astronomy and Informatics, Nicolaus Copernicus University, ul. Grudziądzka 5, 87-100 Toruń, Poland
e-mail:
[2] Astronomical Observatory of the Jagiellonian University, ul. Orla 171, 30-244 Kraków, Poland
[3] Centre for Star and Planet Formation, Niels Bohr Institute and Natural History Museum of Denmark, University of Copenhagen, Øster Voldgade 5-7, DK-1350 Copenhagen K, Denmark
[4] Faculty of Physics, University of Warsaw, ul. Pasteura 5, 02-093 Warszawa, Poland
[5] National Centre for Nuclear Research, ul. Pasteura 7, 02-093 Warszawa, Poland
[6] Nicolaus Copernicus Astronomical Center, ul. Rabiańska 8, 87-100 Toruń, Poland
[7] Leiden Observatory, Leiden University, P.O. Box 9513, NL-2300RA Leiden, The Netherlands

Received [Month] [Day], 2019; accepted [Month] [Day], 2019

ABSTRACT

Aims.
Methods.
Results.

Key words. astrochemistry – stars: formation – ISM: molecules – ISM: individual objects: Sepens Main – Submillimeter: ISM

1. Introduction

2. Observations

2.1. IRAM data and reduction process

The Serpens Main star forming region was observed with IRAM 30 between 14 and 17 July 2009 (project no. xxx, PI: L. Kristensen). We used the Eight MIxer Receiver (EMIR) as the frontend. The observations were performed in the EMIR bands E090 (molecule HCN $J = 1 - 0$) covering the range 73-117 GHz and E150 (molecules CN $J = 1 - 0$ and CS $J = 3 - 2$) covering the frequencies between 125 and 184 GHz. Due to the EMIR receiver wide bands additional molecular lines of $C^{34}S$ $J = 3 - 2$, $H^{13}CN$ $J = 1 - 0$ and $H^{13}CN$ $J = 2 - 1$ were also observed. The backend was the Versatile SPectrometer Array (VESPA) autocorrelator and the 1 MHz filterbank reaching the spectral resolution of 39 kHz (E150 band) and 78 kHz (E090 band). The telescope beam size varies from 14″ at 172.68 GHz to 29″ at 86.34 GHz (Table 1). The antenna temperatures were converted to main-beam brightness temperature $T_{\rm MB}$ using the main beam efficiency according to the expresion: $T_{\rm MB} = T_{\rm A}/\eta_{\rm MB}$. The exact upper levels enegies, line frequencies, beam sizes and beam efficiencies are given in Table 1. Observations included scans of the Ser-SMM1 (centered at $\alpha_{\rm J2000} = 18^h29^m49.6^s$, $\delta_{\rm J2000} = +01°15'20.5''$ with $V_{\rm LSR} = +8.5$ km/s) and the Ser-SMM3/Ser-SMM4 (centered at $\alpha_{\rm J2000} = 18^h29^m56.6^s$, $\delta_{\rm J2000} = +01°14'00.3''$ with $V_{\rm LSR} = +7.6$ km/s) regions, both 1′×3′ OTF maps. The size of the maps is about 300″ × 350″, covering both Ser-SMM1 and Ser-SMM3/Ser-SMM4 regions. The regions are referenced in the article as 'the Northen part' and 'the Southern part' respectively.

Data reduction was carried out with the CLASS package within GILDAS[1]. Each spectrum was corrected for the baseline shape, the spike channels were removed and the velocity was resampled to a resolution of 0.5 km/s. The baseline fitting of the order of 0 was sufficient for our observations. The rms of extracted spectra values vary from 0.024 K to 0.125 K. Both OTF maps were merged in one map covering 300×350 arcsec. The spectra obtained were exported from the CLASS package and analysed with Python scripts.

2.2. Physical properties of embedded protostars

Ten Class 0/I protostars are present in the observed region. There are deeply embedded sources so the radiation coming from theirs neighbourhood is highly absorbed in the envelopes, then reemitted in the IR range. Envelopes become thinner with time due to outflow-envelope interactions (Arce & Sargent 2006). Class I sources SEDs are dominated by the emission in shorter wavelengths in respect to Class 0 objects. Thus Spectral Energy Distributions (SEDs) allow to estimate the evolutional stage of an object (Andre et al. 1993).

Figure A.1 shows spectral energy distributions for all Class 0/1 protostars in the region (Table 2). The SED plots include the selected literature samples (Dunham et al. 2015) combined with the data from the Herschel Gould Belt survey project (André et al. 2010). The additional Herschel data cover the SED peak, therefore provide a more detailed information allowing to calculate the bolometric temperatures and luminosities of the protostar more precisely.

[1] See http://www.iram.fr/IRAMFR/GILDAS

Table 1: Overview of the observations

Mol.	Trans.	ν (GHz)	E_u/k_B (K)	A_{ul} (s^{-1})	g_u	n_{crit} (cm^{-3})	Beam size ($''$)	Beam eff. η_{MB}
HCN	1-0	88.631602	4.25	2.407×10^{-5}	3	5.0×10^{6} [b]	28	0.81
CN	1-0	113.494921	5.45	1.182×10^{-5}	3	1.1×10^{5} [c]	22	0.78
CS	3-2	146.969029	14.1	6.071×10^{-5}	7	2.6×10^{5} [c]	16	0.74
$C^{34}S$	3-2	144.617109	13.9	7.251×10^{-5} [a]	7	5.84×10^{11} [a]	16	0.74
$H^{13}CN$	1-0	86.342274	4.14	1.512×10^{-5} [a]	3	9.7×10^{6} [b]	29	0.81
$H^{13}CN$	2-1	172.677881	12.43	6.90×10^{-5} [a]	5	1.2×10^{6} [c]	14	0.68

References: Molecular data adopted from LAMDA/JPL databases: [a] calculated for T = 300 K; [b]Jiménez-Donaire et al. 2016, assuming optically thin transition lines for an excitation temperature of 20K; [c]Shirley 2015, assuming optically thin transition lines for an excitation temperature of 50K; [d]Chandra et al. 1995.

Notes. Beam sizes and efficiencies are taken from http://www.iram.es/IRAMES/mainWiki/Iram30mEfficiencies

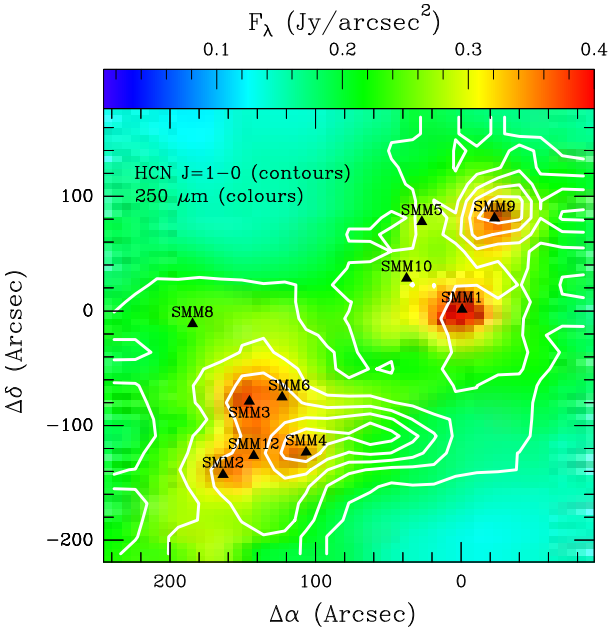

Fig. 1: Molecular emission of HCN J=1-0 (contours) overplot on continuum emission *Herschel*/SPIRE (Griffin et al. 2010) 250 μm (colours). Countours the lowest level is set on 0.4 K km/s (30 σ), step size of 4 K km/s.

Table 2 contains the observed protostars parameters as well as the classification from Enoch et al. 2009. Early Class 0 was defined as a protostar of bolometric temperature lesser than 50 K. Prostostars characterised by bolometric temperature between 50 K and 100 K were classified as Late Class 0 protostars. Class I protostars were divided for Early and Late sub-type by the bolometric temperature of 300 K.

Most of the observed protostars in the Serpens Main region are very young, embedded sources of Early Class 0. SMM4, SMM10 and SMM12 are classified as Late Class 0 YSOs. The SMM5 and SMM6 protostars are the most evolved objects in our sample (Class I).

3. Results

3.1. Molecular emission maps

The line maps in the targeted molecules show variety of structures that can be associated with YSOs and a large-scale cloud emission. Different spatial extend in molecules radiation is connected with various physical conditions around protostars. Here, we present the large-scale maps of CS $J = 3-2$, HCN $J = 1-0$ and CN $J = 1-0$. Maps of their isotopologues are shown in the Appendix A.

We present large-scale intensity maps (Fig. 2) of the targeted lines integrated at the level of 3 σ and above. Three of the observed molecules (HCN, CN and $H^{13}CN$) are characterised by hyperfine structure. High resolution spectroscopy allow us to separate the emission from each hyperfine transitions. The integrated intensity maps of the lowest transitions of HCN, CN and $H^{13}CN$ are performed as a sum of all hyperfine splitting components. The maps are centred at $\alpha_{J2000} = 18^h29^m46.6^s, \delta_{J2000} = 01°18'20.5''$.

Most of molecular emission is concentrated in the SE subcluster, where 6 low-mass protostars are located, while the continuum emission peaks in the NW subcluster what is correlated with the other 4 low-mass protostars positions. The most extended structures can be associated with molecular outflows ejected from low-mass protostars (Table 2). Outflows directions were marked based on previous studies in CO transitions CO $J = 3-2$ (Dionatos et al. 2010) and CO $J = 6-5$/CO $J = 3-2$ (Yıldız et al. 2015). Five off-source positions were selected to detailed spectra analysis (Table 3).

The integrated line intensity map of HCN $J = 1-0$ shows extended emission along outflow directions. This is the strongest line among all observed. The emission is slightly correlated with continuum emission. Most of the emission is associated with protostars positions. The HCN $J = 1-0$ gas peaks around Ser-SMM9 and Ser-SMM4 protostars. There is no significant peak around strong submillimetre sources as Ser-SMM1 and Ser-SMM3. The low energy level of HCN (E_u = 4.25 K) with the critical density of 10^6 cm^{-2} traces cold, high-density gas. HCN has previously been shown to be a good tracer of molecular outflows activity (Lee et al. 2014). The HCN $J = 1-0$ line was detected at all protostars positions, although it is weak at the positions of Ser-SMM5, Ser-SMM8 and Ser-SMM10. On the other hand, the HCN $J = 1-0$ emission is particularly strong in Ser-SMM4 blue-shifted outflow (outflow position no. 4). NS elongated structure is present around Ser-SMM1 protostar what was

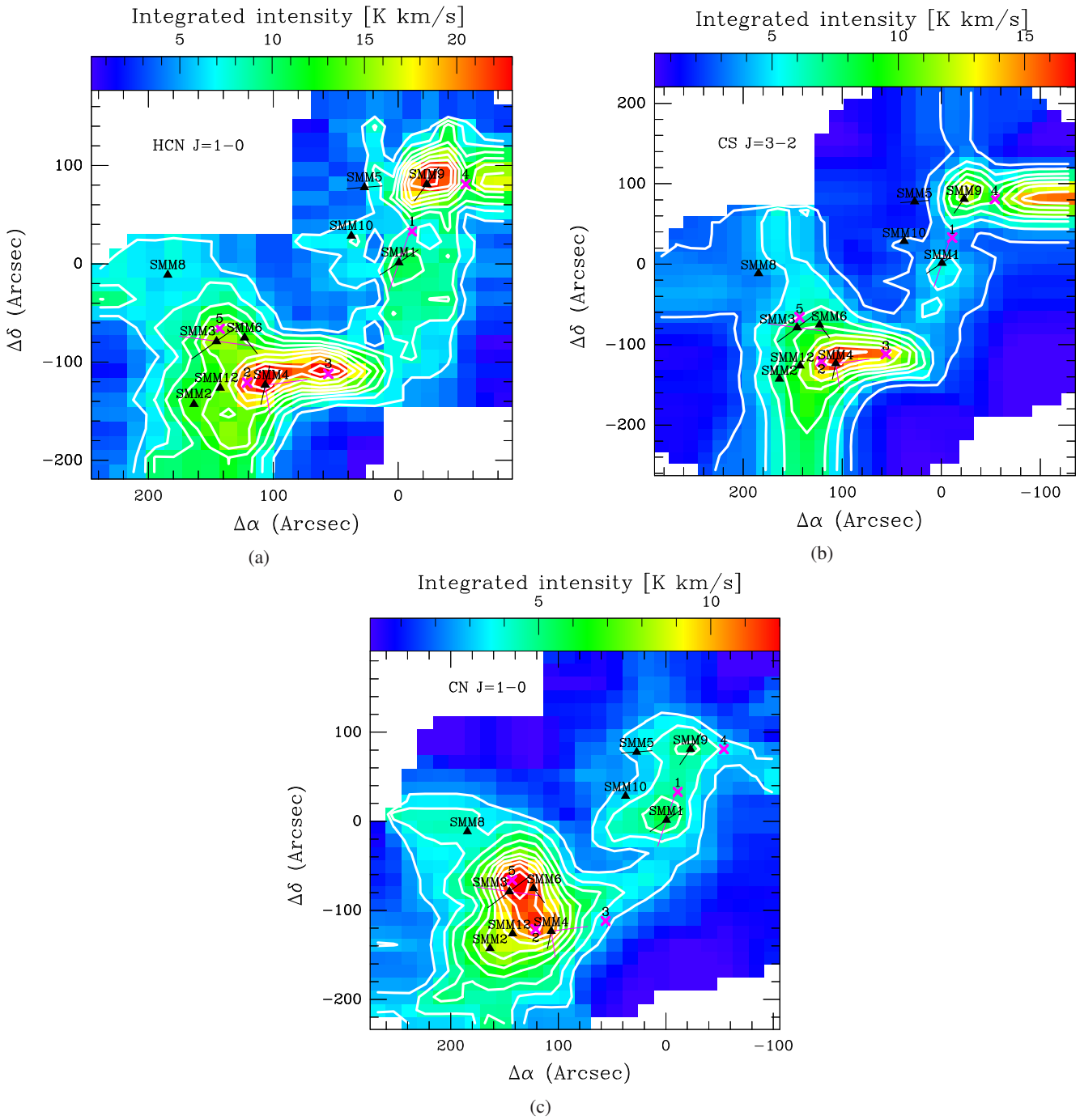

Fig. 2: Integrated intensity $\int T_{\rm mb}\, dV$ of the HCN $J = 1 - 0$ (upper left panel), CS $J = 3 - 2$ (upper right panel) and CN $J = 1 - 0$ (bottom panel) in the Serpens Main region. The first contour at 30 σ level, with step of 10 σ, except CS $J = 3 - 2$ line (b) where the first contour is at 10 σ with step of 5 σ. Black triangles show the positions of the protostars (Suresh et al. 2016), whereas the black lines (Yıldız et al. 2015) and magneta line (Dionatos et al. 2010) show the associated outflow directions. Outflow positions are displayed as magneta crosses.

noticed also in high-J transitions (Yıldız et al. 2015). The emission is slightly extended along Ser-SMM9 outflows. There is no intensively elongated outflow structure from the other sources.

CS $J = 3 - 2$ line emission map shows similar spatial distribution to HCN $J = 1 - 0$. Both species trace the gas of the same properties, however the CS molecule is excited in slightly less dense environment ($\sim 10^5$ cm^{-3}). The most significant elongated structure can be associated with Ser-SMM4 blue-shifted outflow. It is situated at the same place in both maps, extending over 80″. A similar large-scale structure is detected along Ser-SMM1 outflows, although it is stronger in the HCN $J = 1 - 0$ map. Emission around Ser-SMM9 have a circular shape, however, there is additional elongated structure in CS $J = 3 - 2$ line emission towards West. It overlaps with the S68N outflows seen in methanol observations (Kristensen et al. 2010). The HCN $J = 1 - 0$ line emission propagates for larger distances than the CS $J = 3 - 2$. It is also relatively stronger. In both cases the highest peak of the emission is situated around Ser-SMM4 protostar with a signifi-

Table 2: Catalogue of protostars properties

Source (J2000.0)	R.A. (J2000.0)	Decl.	T_{bol} (K)	L_{bol} ($L_\odot$)	Class	Other names
SMM9	18 29 48.3	+01 16 42.7	34.9	10.3	Early Class 0	Ser-emb8, ISO241, WMW23, Bolo22
SMM1	18 29 50.0	+01 15 20.3	35.4	78.7	Early Class 0	Ser-emb6, FIRS1, EC41, Bolo23
SMM5	18 29 51.4	+01 16 38.3	150.5	3.7	Early Class I	Ser-emb21, EC53, WMW24, Bolo22
SMM10	18 29 52.3	+01 15 48.8	82.6	6.2	Late Class 0	Ser-emb12, WMW21, Bolo 23
SMM4	18 29 57.0	+01 13 11.3	76.9	4.4	Late Class 0	Ser-emb22, Bolo25
SMM6	18 29 57.8	+01 14 05.3	532.3	43.1	Late Class I	Ser-emb30, EC90, WMW35, SVS20S, Bolo 28
SMM12	18 29 59.1	+01 13 14.3	96.9	5.7	Late Class 0	Ser-emb19, Bolo28
SMM3	18 29 59.6	+01 13 59.2	35.0	6.9	Early Class 0	Ser-emb26, Bolo26
SMM2	18 30 00.5	+01 12 57.8	30.5	4.07	Early Class 0	Ser-emb4, Bolo28
SMM8	18 30 01.9	+01 15 09.2	15.3	0.2	Early Class 0	Bolo30

Coordinates taken from Suresh et al. 2016, except SMM8 (Lee et al. 2014).

Table 3: Properties of the selected off-source positions

Pos.	R.A. (J200)	Decl. (J200)	Remarks
1	18:29:45.47	+01:15:53.5	SMM1 blue-shifted outflow in CO $J = 3-2$
2	18:29:54.66	+01:13:19.5	max. CN $J = 1-0$, SMM4 blue-shifted outflow in CO $J = 3-2$
3	18:29:50.33	+01:13:68.5	max. HCN $J = 1-0$, SMM4 blue-shifted
4	18:29:43	+01:16:41.5	outflow visible in $C^{34}S$(3-2)
5	18:29:56.13	+01:14:14.5	max. CN $J = 1-0$, SMM9 surroundings

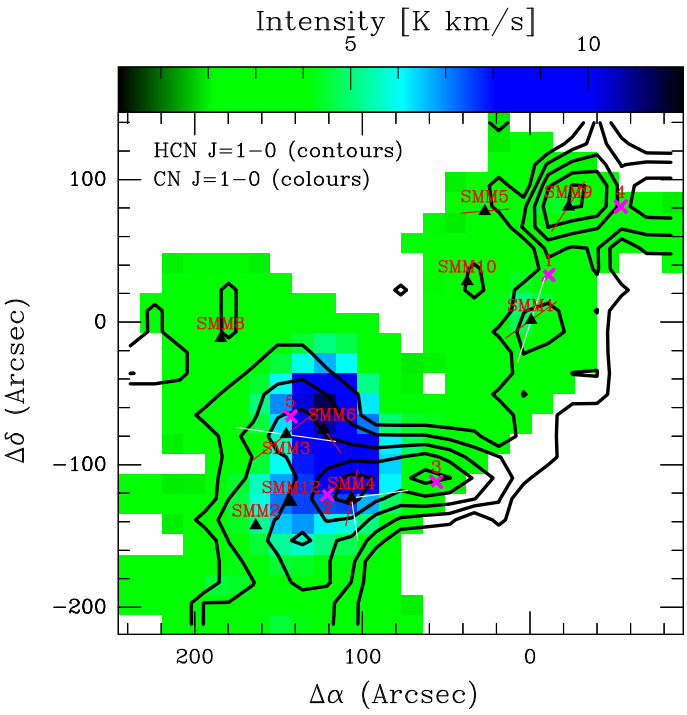

Fig. 3: Integrated intensity $\int T_{mb}\, dV$ of CN $J = 1-0$ (colours) and HCN $J = 1-0$ (contours) in the Serpens Main region. The first contour is 30. Triangles and lines marked as decribed in 2.

cant extent towards outflow position no. 3. Their weaker isotopic species $H^{13}CN$ $J = 1-0$ and $C^{34}S$(3-2) lines peak around the protostars position. The lines exhibits similar morphological distribution as HCN $J = 1-0$ and CS $J = 3-2$.

CN $J = 1-0$ line emission is focused mostly around the positions of protostars. The CN line is similarly low-energetic, however it peaks in different areas than HCN and CS. The CN $J = 1-0$ integrated intensity structures follow the 250 μm continuum map. The highest local peaks are associated with Class 0 low-mass protostars: Ser-SMM3, Ser-SMM4 and Ser-SMM6, as well as local maxima around Ser-SMM1 and Ser-SMM9. The spatial distribution is qualitatively different compared to the HCN $J = 1-0$ and CS $J = 3-2$ maps. The strongest emission characterises the dense surroundings of protostars in SE subcluster while the NW subcluster does not show such a distinct emission as in the HCN $J = 1-0$ line. Dense emissive region of the Ser-SMM9 source is significantly weaker in CN $J = 1-0$ line. CN $J = 1-0$ map can be characterised by compact, condensed emission without any strongly elongated structures.

3.2. Line profiles

We selected 14 representative on-source and off-source positions for a detailed analysis (Fig. **??**). Nine of them are corresponding to the protostars positions, the other five off-source positions were selected based on local maximum of the flux.

In the majority of our sources five of targeted lines were detected: CN $J = 1-0$, HCN $J = 1-0$, CS $J = 3-2$, $C^{34}S$ $J = 3-2$ and $H^{13}CN$ $J = 1-0$. The line is considered to be detected if there is an emission at the level of at least 3σ. A weak emission from $H^{13}CN$ $J = 2-1$ was found at the positions of four sources and it is not included in Fig. **??**.

The strongest emission occurs in HCN $J = 1-0$, CN $J = 1-0$ and CS $J = 3-2$ lines and it was detected at the position of all of the sources. The emission in the other lines was multiplied in order to compare profiles between different molecules. In HCN, CN species and their isotopologues a few different velocity components can be identified what indicates the hyperfine splitting. This occurs if a molecule has a non-zero nuclear spin so there is also an interaction between the nuclear spin and the electronic angular momentum. The most distinct splitting can be spotted in the CN $J = 1-0$ profiles with five separate components situated between -70 km/s and 18 km/s. The HCN $J = 1-0$ line is characterised by three components with low separation situated in the range of -2 km/s – 16 km/s.

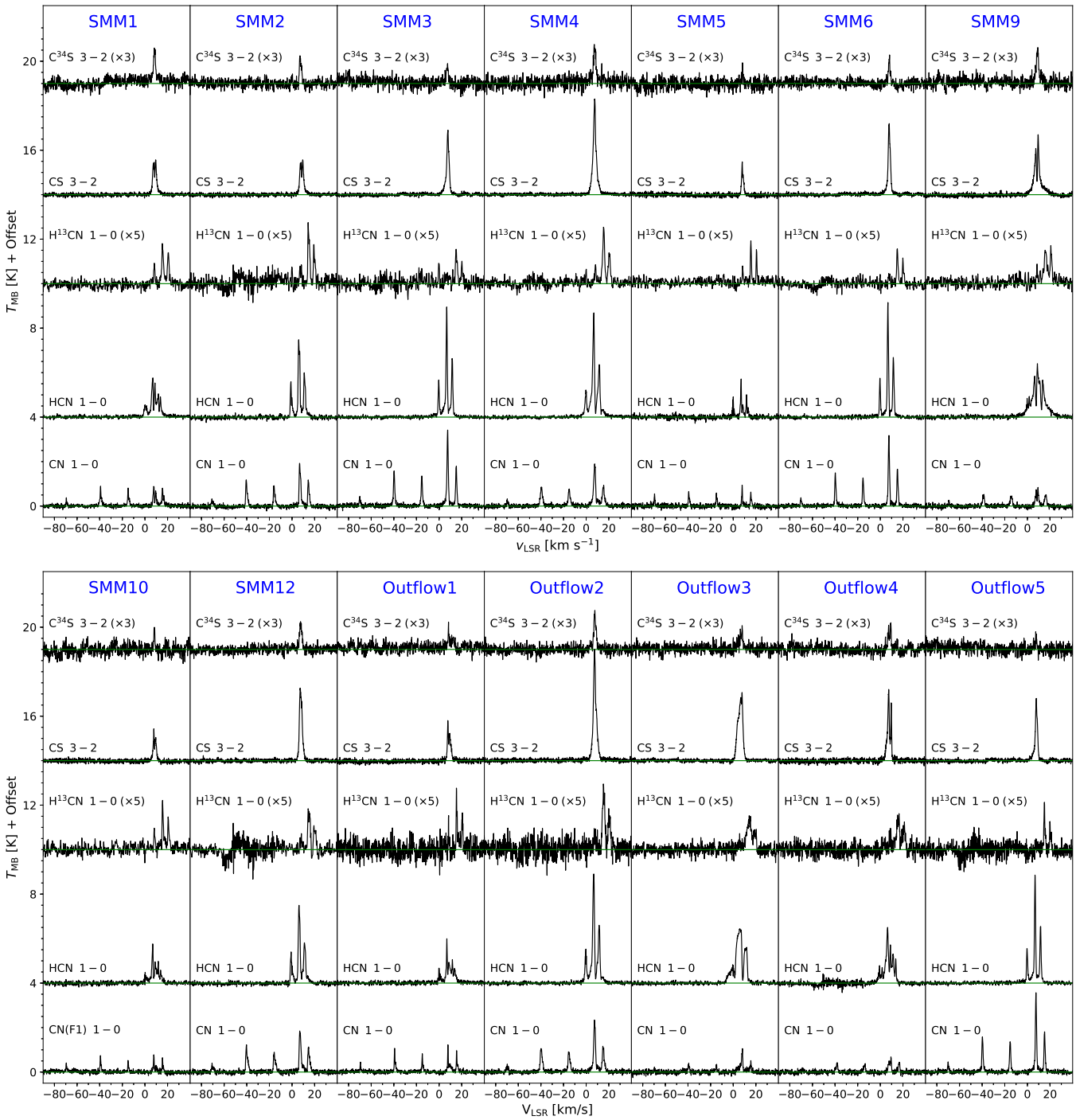

Fig. 4: Serpens Main sources spectra of $C^{34}S$ $J = 3 - 2$, CS $J = 3 - 2$, $H^{13}CN$ $J = 1 - 0$, HCN $J = 1 - 0$ and CN $J = 1 - 0$ lines.

Ser-SMM1, Ser-SMM9, and Ser-SMM10 sources have wide spectral lines, while others exhibit narrow line profiles. Spectra extracted form Outflows no. 1, 4 and 5 shows prominent blue-shifted wings. Similar structure can be noticed in the Ser-SMM3 (panel no. 7) CS 3-2 and HCN $J = 1 - 0$ profiles.

4. Analysis

5. Discussion

6. Conclusions

Acknowledgements. AM, AK and MG are supported by the Polish National Science Center grants NAVA InterAPS and 2016/21/D/ST9/01098. This research has made use of data from the Herschel Gould Belt survey (HGBS) project (http://gouldbelt-herschel.cea.fr). The HGBS is a Herschel Key Programme jointly carried out by SPIRE Specialist Astronomy Group 3 (SAG 3), scientists of several institutes in the PACS Consortium (CEA Saclay, INAF-IFSI Rome and INAF-Arcetri, KU Leuven, MPIA Heidelberg), and scientists of the Herschel Science Center (HSC).

Table 4: Integrated fluxes of the observed line at the positions of protostars

Source	Line	$\int T_{mb}\,dV$ (K km/s)	T_{peak} (K)	N_{up} (cm^{-2})	N_{tot} (cm^{-2})
SMM1	CN 1-0	5.26	0.89	1.1×10^{13}	6.6×10^{14}
	HCN 1-0	8.23	1.76	5.2×10^{12}	2.0×10^{14}
	CS 3-2	2.98	1.57	2.1×10^{12}	2.3×10^{13}
	$C^{34}S$ 3-2	1.21	0.56		
	$H^{13}CN$ 1-0	1.43	0.45		
SMM2	CN 1-0	8.41	1.92	1.8×10^{13}	1.1×10^{15}
	HCN 1-0	12.57	3.48	8.0×10^{12}	3.0×10^{14}
	CS 3-2	6.57	3.10	4.5×10^{12}	2.0×10^{13}
	$C^{34}S$ 3-2	0.89	0.47		
	$H^{13}CN$ 1-0	1.65	0.64		
SMM3	CN 1-0	13.18	3.42	2.8×10^{13}	1.7×10^{15}
	HCN 1-0	14.14	4.95	8.9×10^{12}	3.4×10^{14}
	CS 3-2	8.11	2.90	5.6×10^{13}	6.2×10^{13}
	$C^{34}S$ 3-2	0.604	0.36		
	$H^{13}CN$ 1-0	0.88	0.41		
SMM4	CN 1-0	9.89	1.90	2.1×10^{13}	1.3×10^{15}
	HCN 1-0	17.59	4.69	1.1×10^{13}	4.2×10^{14}
	CS 3-2	14.4	4.30	9.9×10^{12}	1.1×10^{14}
	$C^{34}S$ 3-2	1.56	0.64		
	$H^{13}CN$ 1-0	1.83	0.61		
SMM5	CN 1-0	3.49	0.94	7.3×10^{12}	4.4×10^{14}
	HCN 1-0	5.79	1.72	3.7×10^{12}	1.4×10^{14}
	CS 3-2	2.61	1.48	1.8×10^{12}	2.0×10^{13}
	$C^{34}S$ 3-2	0.28	0.42		
	$H^{13}CN$ 1-0	1.16	0.42		
SMM6	CN 1-0	10.57	3.17	2.2×10^{13}	1.3×10^{15}
	HCN 1-0	11.85	5.15	8.9×10^{12}	3.3×10^{14}
	CS 3-2	7.86	3.2	5.4×10^{12}	6.0×10^{13}
	$C^{34}S$ 3-2	0.74	0.56		
	$H^{13}CN$ 1-0	0.81	0.40		
SMM8	CN 1-0	5.09	0.94	1.1×10^{13}	6.4×10^{14}
	HCN 1-0	6.32	1.72	4.0×10^{12}	1.5×10^{14}
	CS 3-2	4.64	2.08	3.2×10^{12}	3.5×10^{13}
	$C^{34}S$ 3-2	0.22	0.35		
	$H^{13}CN$ 1-0	0.46	0.21		
SMM9	CN 1-0	5.41	0.84	1.1×10^{13}	6.8×10^{14}
	HCN 1-0	14.08	2.40	8.9×10^{12}	3.4×10^{14}
	CS 3-2	9.85	2.70	6.8×10^{12}	7.5×10^{13}
	$C^{34}S$ 3-2	1.3	0.62		
	$H^{13}CN$ 1-0	1.57	0.38		
SMM10	CN 1-0	2.59	0.78	5.4×10^{12}	3.3×10^{14}
	HCN 1-0	6.96	1.75	4.4×10^{12}	1.7×10^{14}
	CS 3-2	3.83	1.43	2.6×10^{12}	2.9×10^{13}
	$C^{34}S$ 3-2	0.56	0.40		
	$H^{13}CN$ 1-0	0.98	0.45		
SMM12	CN 1-0	9.10	1.85	1.9×10^{13}	1.2×10^{15}
	HCN 1-0	13.27	3.50	8.4×10^{12}	3.2×10^{14}
	CS 3-2	9.75	3.26	6.7×10^{12}	7.4×10^{13}
	$C^{34}S$ 3-2	1.18	0.58		
	$H^{13}CN$ 1-0	1.43	0.46		

References

André, P., Men'shchikov, A., Bontemps, S., et al. 2010, A&A, 518, L102
Andre, P., Ward-Thompson, D., & Barsony, M. 1993, ApJ, 406, 122
Arce, H. G. & Sargent, A. I. 2006, ApJ, 646, 1070
Aso, Y., Hirano, N., Aikawa, Y., et al. 2018, ApJ, 863, 19
Di Francesco, J., Johnstone, D., Kirk, H., MacKenzie, T., & Ledwosinska, E. 2008, ApJS, 175, 277
Dionatos, O., Nisini, B., Codella, C., & Giannini, T. 2010, A&A, 523, A29
Dunham, M. M., Allen, L. E., Evans, Neal J., I., et al. 2015, ApJS, 220, 11
Enoch, M. L., Evans, Neal J., I., Sargent, A. I., & Glenn, J. 2009, ApJ, 692, 973
Enoch, M. L., Glenn, J., Evans, Neal J., I., et al. 2007, ApJ, 666, 982

Table 5: Patterns of emission in molecular spieces

Source	HCN $J = 1 - 0$	CN $J = 1 - 0$	Remarks
SMM1	rb	c	multiple system of 5 components[a]
SMM2	b	b	multiple system of 3 components[b]
SMM3	b	b	
SMM4	rb	rb	binary[c]
SMM5	x	x	variable[d]
SMM5	x	x	
SMM8	r	r	
SMM9	rb	r	
SMM10	x	x	
SMM12	b	b	

References: *a* Hull et al. (2017), *b* Francis et al. (2019), [c] Aso et al. (2018), [d] Yoo et al. (2017).

Evans, Neal J., I., Dunham, M. M., Jørgensen, J. K., et al. 2009, ApJS, 181, 321
Francis, L., Johnstone, D., Dunham, M. M., Hunter, T. R., & Mairs, S. 2019, ApJ, 871, 149
Hull, C. L. H., Girart, J. M., Tychoniec, Ł., et al. 2017, ApJ, 847, 92
Kristensen, L. E., van Dishoeck, E. F., van Kempen, T. A., et al. 2010, A&A, 516, A57
Lee, K. I., Fernández-López, M., Storm, S., et al. 2014, ApJ, 797, 76
Myers, P. C. & Ladd, E. F. 1993, ApJ, 413, L47
Ortiz-León, G. N., Dzib, S. A., Kounkel, M. A., et al. 2017, ApJ, 834, 143
Skrutskie, M. F., Cutri, R. M., Stiening, R., et al. 2006, AJ, 131, 1163
Suresh, A., Dunham, M. M., Arce, H. G., et al. 2016, AJ, 152, 36
Wright, E. L., Eisenhardt, P. R. M., Mainzer, A. K., et al. 2010, AJ, 140, 1868
Yıldız, U. A., Kristensen, L. E., van Dishoeck, E. F., et al. 2015, A&A, 576, A109
Yoo, H., Lee, J.-E., Mairs, S., et al. 2017, ApJ, 849, 69

Appendix A: Spectral Energy Distributions

Broad-band observations are needed in order to determine physical properties of a protostar. Dunham et al. 2015 studied properties of protostars in the Serpens molecular cloud using 2MASS (Skrutskie et al. 2006) and Spitzer IRAC/MIPS (Evans et al. 2009), observations covering the range of 1.25–70 μm, photometry from Wide-field Infrared Survey Explorer 12 and 22 μm (WISE; Wright et al. 2010), SHARC-II 350 μm (Suresh et al. 2016), the SCUBA Legacy Catalog 450 and 850 μm (Di Francesco et al. 2008) and 1.1 mm observations from Bolocam dust survey (Enoch et al. 2007). The Serpens Main region was also observed during the Herschel Gould Belt survey project (André et al. 2010). SPIRE/PACS photometry in the Serpens molecular cloud is discussed in Fiorellino et al. (in prep.).

Based on SEDs the bolometric temperature and luminosity can be calculated for each of the observed protostars. The bolometric luminosity was determined by integrating the SEDs over frequency:

$$L_{bol} = \pi\, d^2 \int F_\nu d\nu \tag{A.1}$$

where d is the cloud distance of 436 ± 9.2 pc (Ortiz-León et al. 2017). The bolometric temperature was calculating as described in Myers & Ladd 1993:

$$T_{bol} = 1.25\, 10^{-11}\, \bar{\nu} \tag{A.2}$$

where $\bar{\nu}$ is the mean frequency given by:

$$\bar{\nu} = \frac{\int \nu F_\nu d\nu}{\int F_\nu d\nu} \tag{A.3}$$

Using Scipy *splrep* and *splev* functions cubic smooth spline interpolation of the photometric data was performed while calculating the protostars parameters. Integration along the resulting axis was obtain with the composite trapezoidal rule (*Scipy* package). The photometric data allows us to perform the integration along wide range of wavelength with exception of SMM8. Here we have only 4 photometric points from the Herschel Gould Belt so the calculeted bolometric luminosity and temperature can be underestimated.

Appendix B: Molecular emission maps

Appendix C: Flux correlations

Appendix D: Wings emission

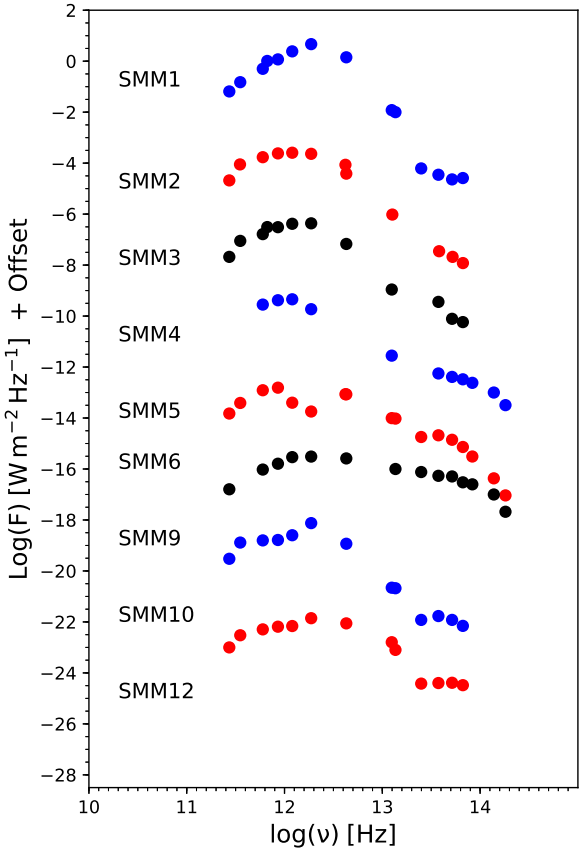

Fig. A.1: Spectral Energy Distributions of protostars in the Serpens Main region.

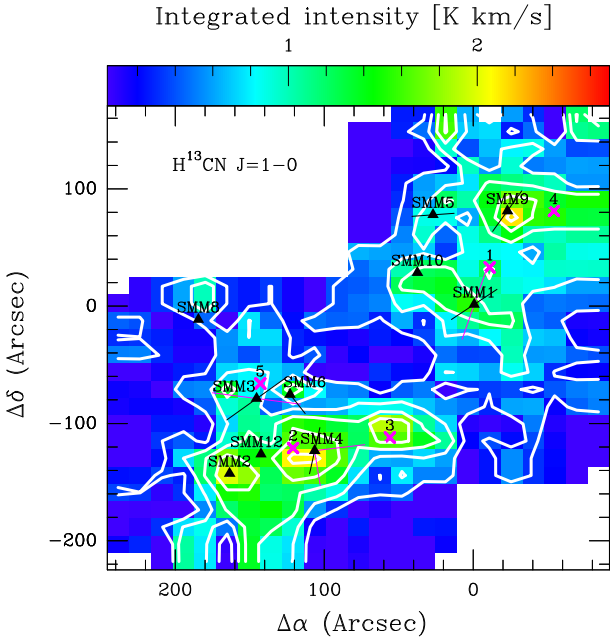

Fig. B.1: Similar to Fig. 2 but the emission of the H^{13}CN $J = 1 - 0$ line. The first contour at 10 σ level, with step of 10 σ

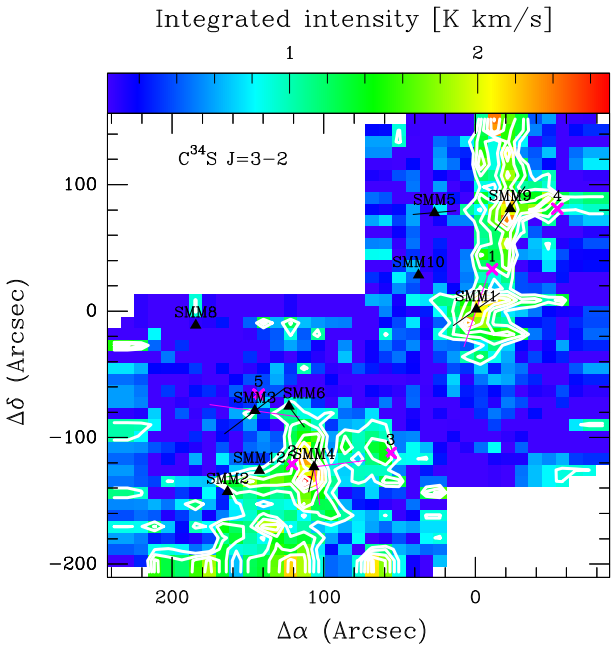

Fig. B.2: Similar to Fig. 2 but the emission of the $C^{34}S$ $J = 3 - 2$ line. The first contour at 30 σ level, with step of 10 σ

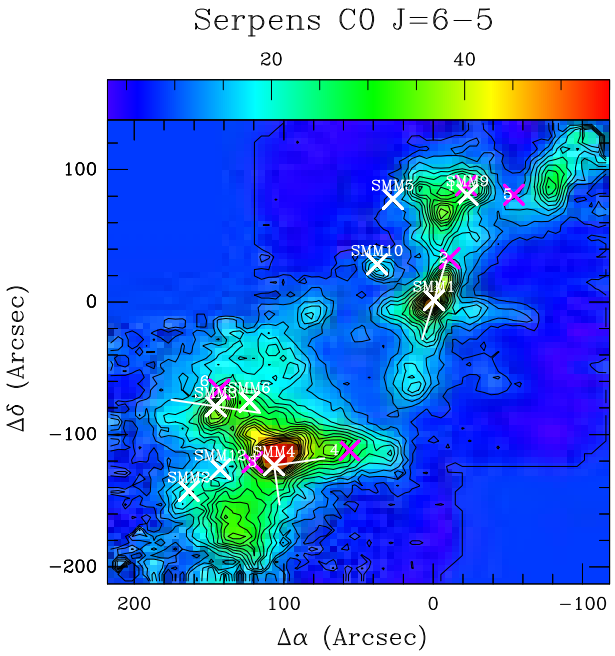

Fig. B.3: APEX map: the emission of the CO $J = 6 - 5$ line.

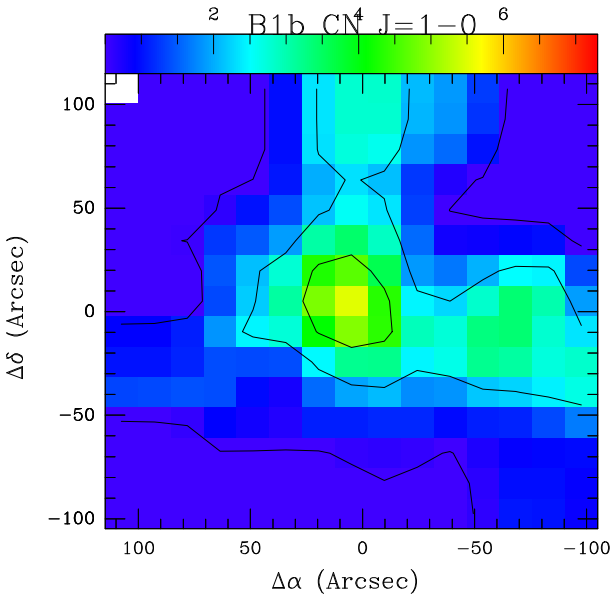

Fig. B.4: Similar to Fig. 2 but the emission of the CN $J = 1 - 0$ line in B1-b region.

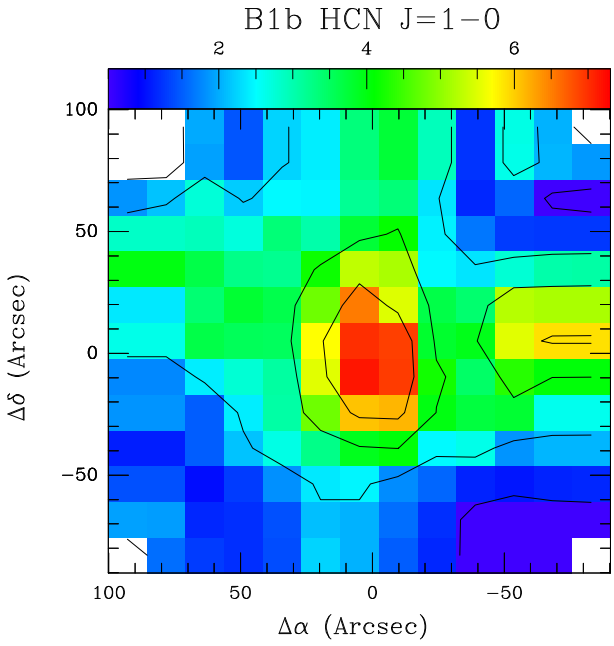

Fig. B.5: Similar to Fig. 2 but the emission of the HCN $J = 1 - 0$ line in B1-b region.

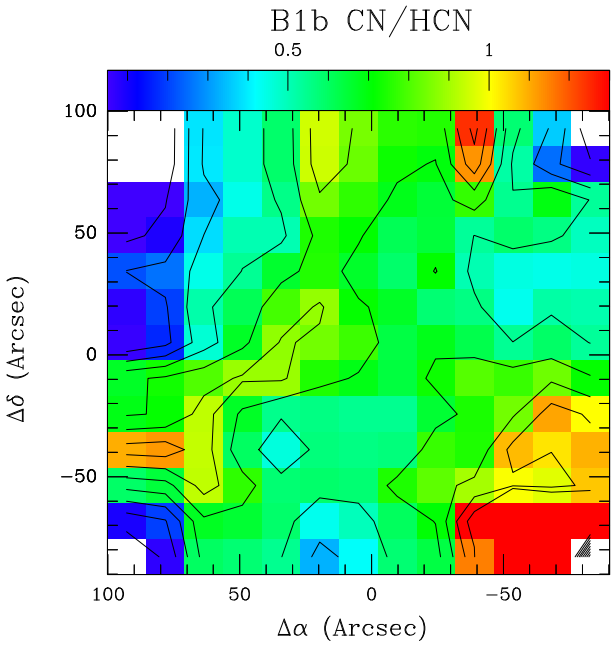

Fig. B.6: Similar to Fig. 2 but the emission of the CN/HCN in B1-b region.

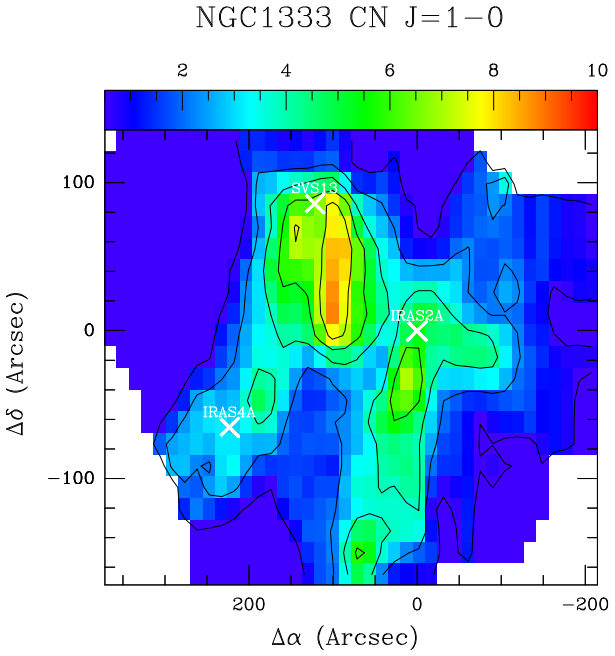

Fig. B.7: Similar to Fig. 2 but the emission of the CN $J = 1 - 0$ line in NGC1333 region.

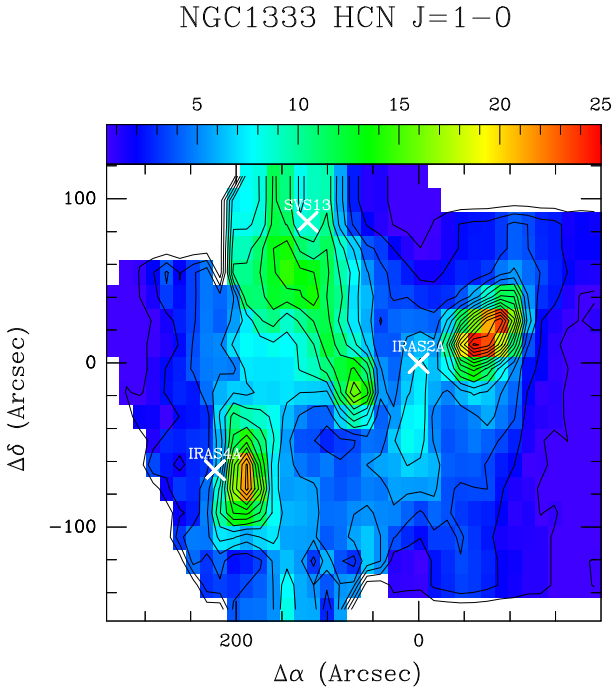

Fig. B.8: Similar to Fig. 2 but the emission of the HCN $J = 1 - 0$ line in NGC1333 region.

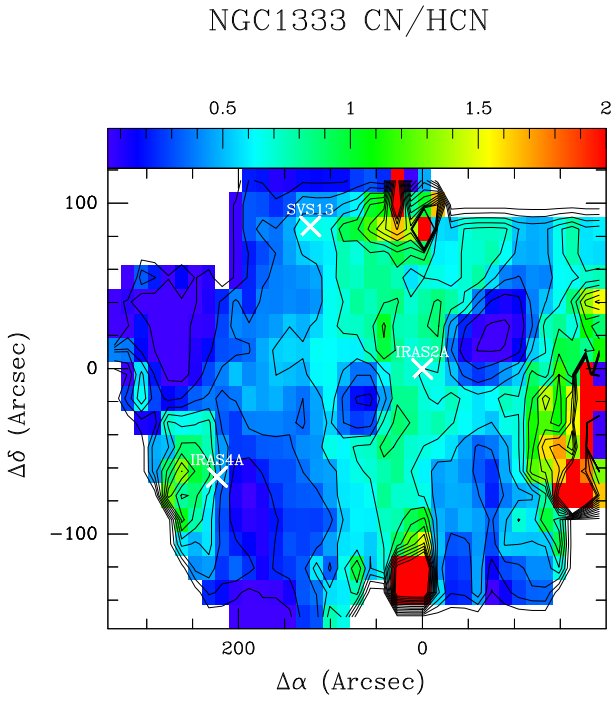

Fig. B.9: Similar to Fig. 2 but the emission of the CN/HCN in NGC1333 region.

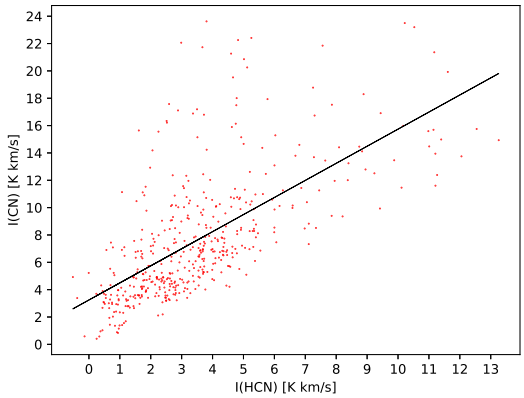

Fig. C.1: Correlation of CN $J = 1 - 0$ and HCN $J = 1 - 0$ integrated intensities $\int T_{mb}\, dV$ for every pixel. A least-squares linear regresion (black line) with following parametes: slope = 1.25, intercept = 0.24, stderr = 0.07. The Pearson correlation coefficient equals 0.65.

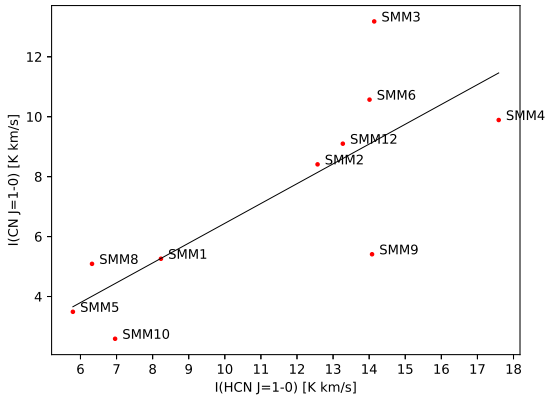

Fig. C.2: Correlation of $CNJ = 1 - 0$ and $HCNJ = 1 - 0$ integrated intensities $\int T_{mb}\, dV$ for all sources. A least-squares linear regresion (black line) with following parametes: slope = 0.66, intercept = -0.17, stderr = 0.18. The Pearson correlation coefficient equals 0.79.

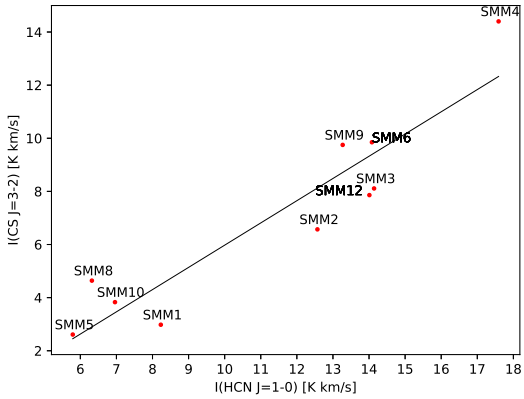

Fig. C.3: Similar to Fig. C.2 but CS $J = 3 - 2$ and HCN $J = 1 - 0$ lines correlation. A least-squares linear regresion (black line) with following parametes: slope = 0.83, intercept = -2.39, stderr = 0.12. The Pearson correlation coefficient equals 0.93.

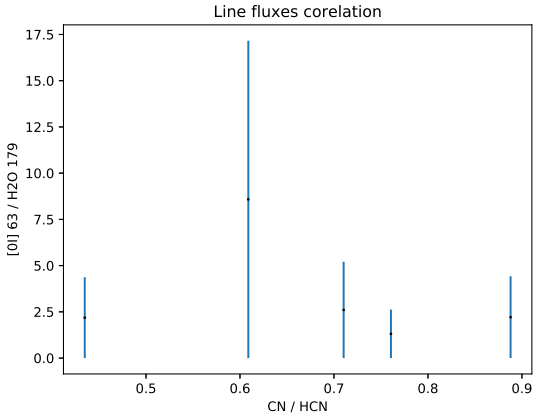

Fig. C.4: Correlation of [OI] 63 μm and H_2O 179 μm fluxes.

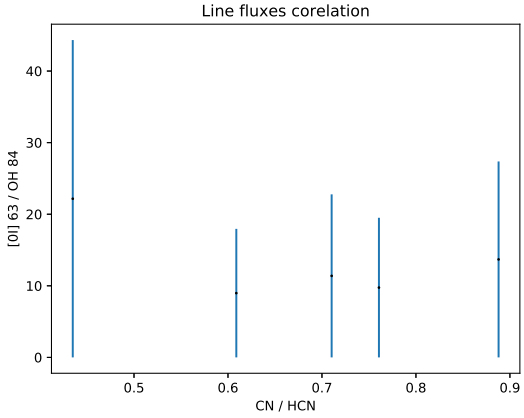

Fig. C.5: Correlation of [OI] 63 μm and OH 84 μm fluxes.

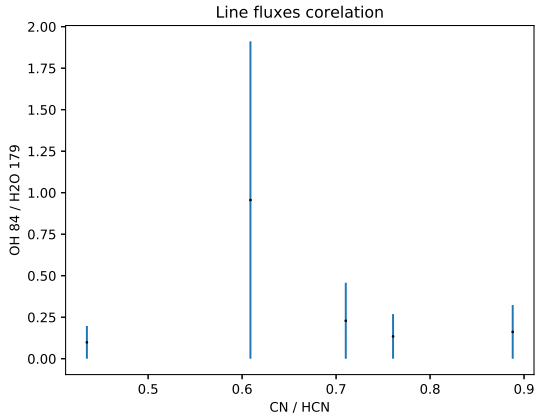

Fig. C.6: Correlation of OH 84 μm and H_2O 179 μm fluxes.

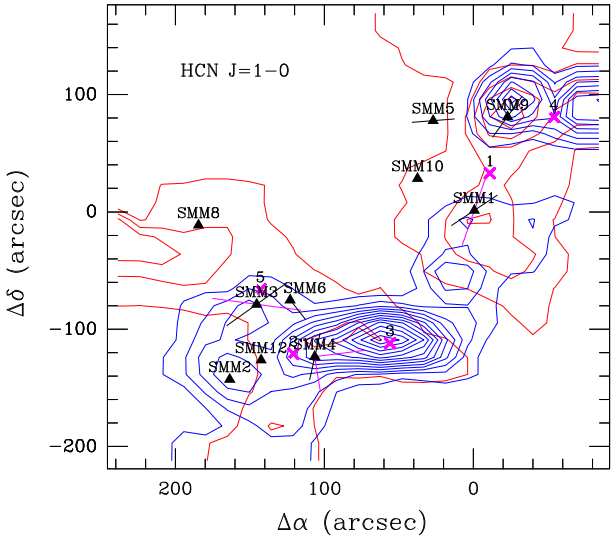

Fig. D.1: HCN $J = 1 - 0$ blue-shifted and red-shifted emission in Serpens Main region. The first contour is at 5 σ with the step of 3 σ. Triangles and lines marked as decribed in 2.

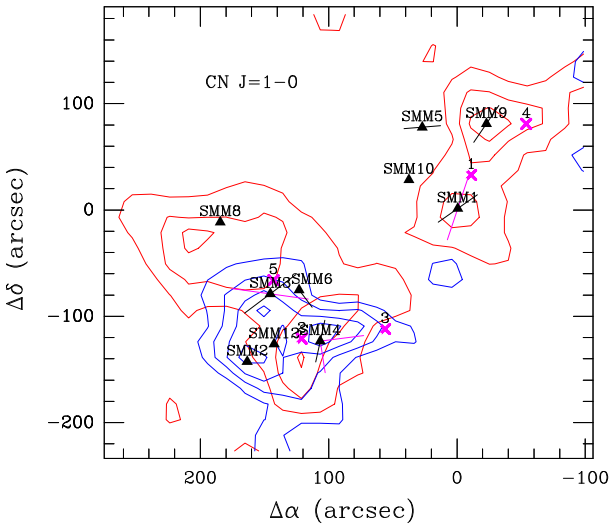

Fig. D.2: Similar to Fig. D.1 but the emission of the CN $J = 1-0$ line.